Stability derivatives for a delta-wing X-31 aircraft validated using wind tunnel test data

N Anton, R M Botez*, and **D Popescu**
Ecole de Technologie Supérieure, Laboratory of Research in Active Controls, Avionics and AeroServoElasticity LARCASE, Montréal, Québec, Canada

The manuscript was received on 24 January 2010 and was accepted after revision for publication on 16 August 2010.

DOI: 10.1243/09544100JAERO799

Abstract: The calculation and validation of the aerodynamic coefficients and stability derivatives for the X-31 model aircraft are the focus of this study. To improve the stability derivative calculations for a delta-wing aircraft in the subsonic regime, a compendium of new methods is programmed into a new code, FDerivatives, and added to the classical DATCOM method. The FDerivatives code is described, as are the improvements achieved in the aircraft canard configuration. All the required geometrical data relative to the aerodynamic coefficient estimation of the X-31 aircraft are calculated for the wing–body–tail configuration. Digital DATCOM code was used to validate the geometry and the aerodynamic coefficients, as well as the implicit method and the Jorgensen method. Experimental results are provided for the X-31 model in the low-speed wind tunnel of the German–Dutch Wind Tunnels (DNW–NWB). The FDerivatives code gives very good results in comparison with experimental results. An analysis of longitudinal motion, based on FDerivatives results, is presented at the end.

Keywords: delta-wing aircraft, stability derivatives, graphical interface, modelling, validation

1 INTRODUCTION

From a methodological perspective, this article discusses a qualitative approach and presents the approaches the authors used to produce a tool for calculating the aerodynamic coefficients and derivatives of stability. One of the most difficult aspects of aircraft development is defining the stability and control characteristics. To predict these characteristics, some tools can be used – wind tunnel tests and flight tests. Flight testing is more accurate, but it is very expensive. Other methods work with models that have different levels of fidelity, such as computational fluid dynamics (CFD) for a non-linear aircraft model.

Several studies have been conducted on the X-31 aircraft. Yeh *et al.* [**1**] performed numerical calculations for pre- and post-stall flight regimes, including variable canard deflection settings, and the numerical results were compared with wind tunnel and flight test data.

Phenomena such as wing rock, spins, and departures, which can dominate the high-alpha behaviour of the X-31 configuration and restrict its usable flight envelope, were identified [**2**] by using dynamic model testing techniques for high angle of attack. The results of these tests have been used to design flight control concepts and configuration modifications to minimize the adverse effects of these phenomena.

The self-induced roll characteristics of a 2 per cent subscale X-31 aircraft model were investigated [**3**]. Some unusual aerodynamic phenomena have emerged during X-31 model testing, namely wing rock and autorotation.

A method for determining the yawing moment asymmetry from flight data was developed along with an analysis of the various configuration changes [**4**]. Several aerodynamic modifications were made to the X-31 forebody with the goal of minimizing the asymmetry. Applying symmetrical boundary-layer transition strips along the forebody sides increased the magnitude of the asymmetry and widened the angle-of-attack range over which the largest asymmetry acted.

**Corresponding author: Ecole de Technologie Supérieure, Laboratory of Research in Active Controls, Avionics and AeroServoElasticity LARCASE, Montréal, Québec, H3C 1K3 Canada.*
email: ruxandra.botez@etsmtl.ca

For the model at scale 1:5.6 tested in the German–Dutch Wind Tunnels (DNW–NWB), very few stability derivative results have been published. Boelens [**5**] presents the results from lift, drag, and pitching moment coefficients and pressure coefficients using the CFD method employing three leading-edge configurations: all leading-edge flap gaps, only the longitudinal flap gaps, and no leading-edge flap gaps.

In this context, the authors chose to use the new code, FDerivatives [**6**, **7**], developed at the LARCASE laboratory, to estimate the aerodynamic coefficients and their corresponding stability derivatives. This code was written in MATLAB language and has a complex structure which contains a graphical interface to facilitate the work of potential users. The static and dynamic derivatives may be estimated based only on knowledge of the aircraft geometry, using the DATCOM method [**8**]. The DATCOM procedure is one of the best compilations of knowledge in the field of analytical calculation of aircraft aerodynamic coefficients and stability derivatives. Designed as a tool for the evaluation of aerodynamic coefficients and stability derivatives for preliminary aircraft design, DATCOM provides methods for making these calculations for various aircraft configurations and different flight regimes, based on the wing geometry. For the main functions of calculation, the implementation of the general model has been developed and applied to all the calculation methods used in the code. This facilitates the replacement of calculation methods, including adding new methods, and simplifies troubleshooting throughout the code. Also, the authors have developed a process for the systematic utilization of various monograms in the DATCOM procedure, incorporating MATLAB's interpolation tools.

After these stability derivatives have been calculated, an aircraft's stability can be determined for longitudinal and lateral motions. This article considers only an aircraft's longitudinal behaviour about the pitch-axis reference frame, presented in the last section. The set of the first-order linear differential equations was solved for short-period and phugoid motions. Numerical results are given as eigenvalues, modal damping, natural frequency, magnitude and phasing, magnitude scaling, and phase angle difference. Time-history traces of the short-period and phugoid responses due to an initial condition of the eigenvector are also presented. The system's control response has been investigated using a step control input for the short-period approximation.

2 FDERIVATIVES CODE DESCRIPTION

The first main advantage of the FDerivatives code [**6**, **7**] developed at the LARCASE laboratory (www.larcase.etsmtl.ca) with respect to the Digital DATCOM code (http://www.pdas.com/datcom.htm) is the estimation of the lift, drag, and moment coefficients and their corresponding stability derivatives by use of a minimum of aircraft geometrical data. These data are the area, aspect ratio, taper ratio, sweepback angle, and dihedral angle for the wing, canard, and vertical tail. In addition, their co-ordinates and body parameters are also determined in the three-dimensional (3D) planes.

The FDerivatives program was written based on MATLAB and has a complex structure which contains a graphical interface to facilitate the work of potential users.

2.1 FDerivatives: logical scheme and graphical interface

Figure 1 shows a brief logical scheme of this code, which works in two steps. The first step is the preprocessing level, in which the geometry is completely calculated based on initial characteristics such as the length and the gravity centre position for the fuselage and the reference area, and on the span, aspect ratio, mean aerodynamic chord (MAC), thickness ratio, leading-edge sweep (inboard/outboard), semi-span of exposed surface, root chord, tip chord, and MAC for the wing, canard, and vertical tail. During the second step, the aerodynamic coefficients (lift, drag, and normal and pitching moment coefficients) for different flight conditions are calculated. The accuracy of these four aerodynamic coefficients directly influences the calculation of stability derivatives.

The graphical interface (Figs 2 to 5) allows users to easily and rapidly change the aircraft geometrical data for different flight conditions (for the same aircraft configuration, it will be possible to change only the geometry).

The principle images of the graphical interface are shown for the main window (Fig. 2), wing, and canard parameters (Fig. 3); fuselage parameters (Fig. 4); and vertical tail parameters (Fig. 5). The results obtained for the Hawker 800XP aircraft, and thus for a classical wing–body–tail aircraft, were presented [**6**]. To obtain the results presented in this article for the X-31 aircraft, the code and graphical interface for the Hawker 800XP [**6**] were changed, due to the canard configuration, and therefore new functions were added. The FDerivatives code can also be used for a non-straight-tapered (double trapezoidal) wing, and not just for a straight-tapered wing configuration (see Fig. 3).

In the main window, entitled stability derivatives (Fig. 2), the configuration type and the flight conditions (Mach numbers, altitudes, and angle-of-attack ranges) are defined. It is possible to fix the wing position and its roughness. For each of the three major surfaces (wing, canard, and vertical tail), the global

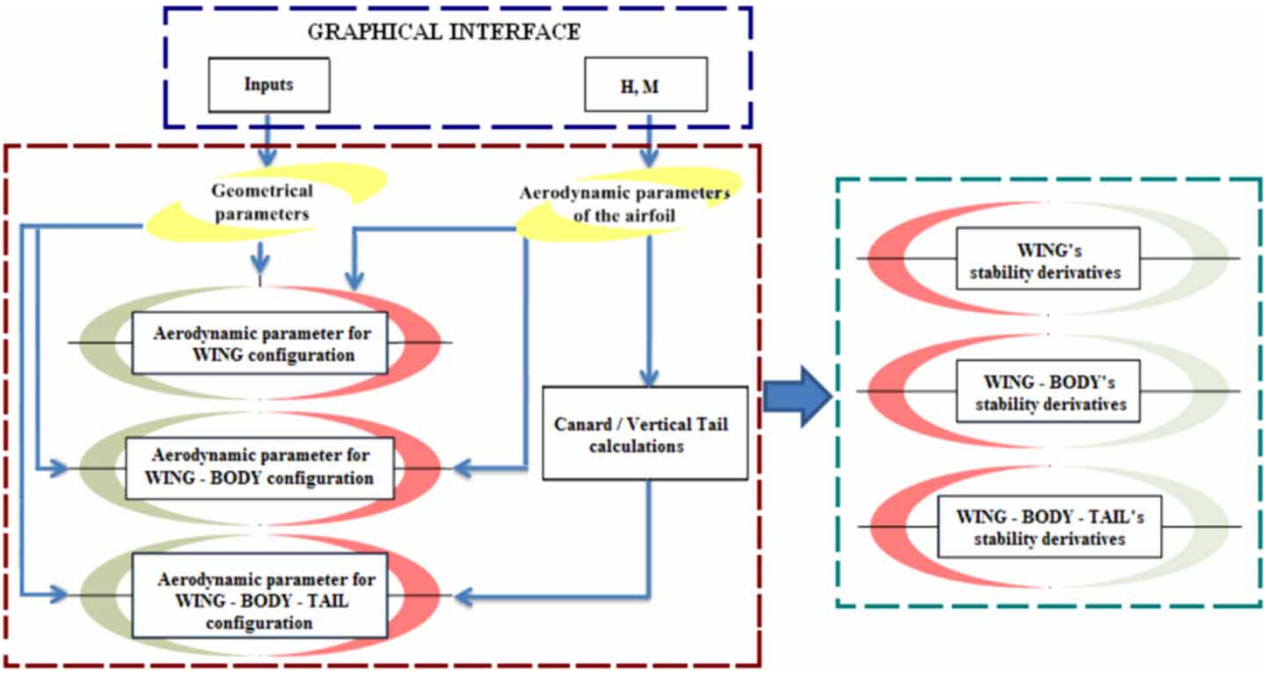

Fig. 1 FDerivatives' logical scheme

Fig. 2 Main window

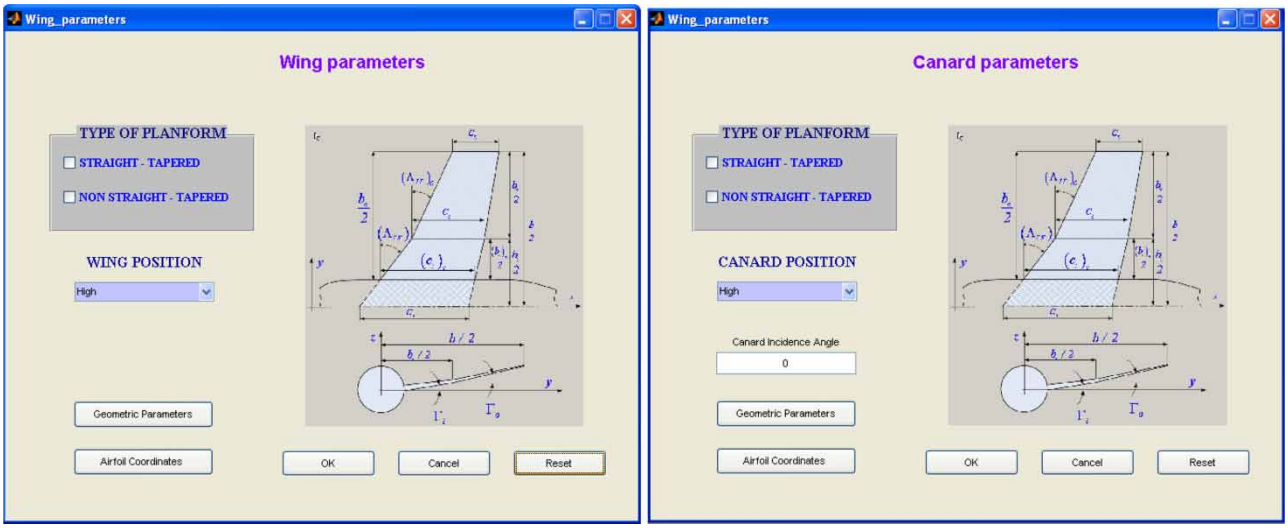

Fig. 3 Wing and canard parameters

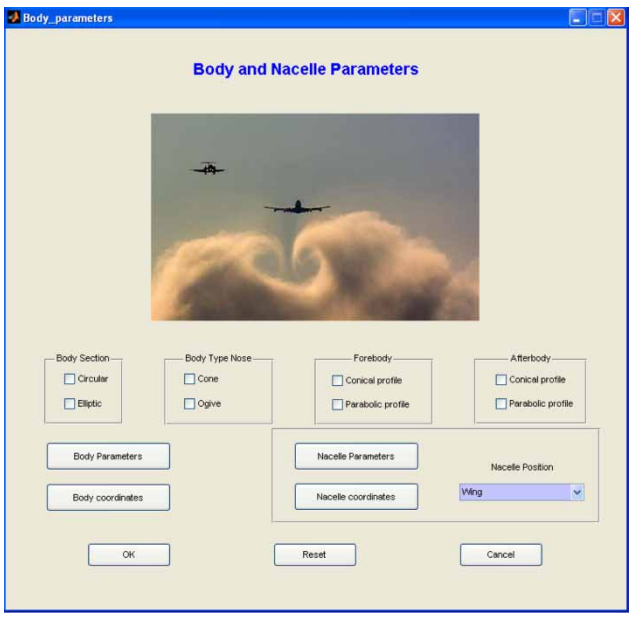

Fig. 4 Fuselage parameters

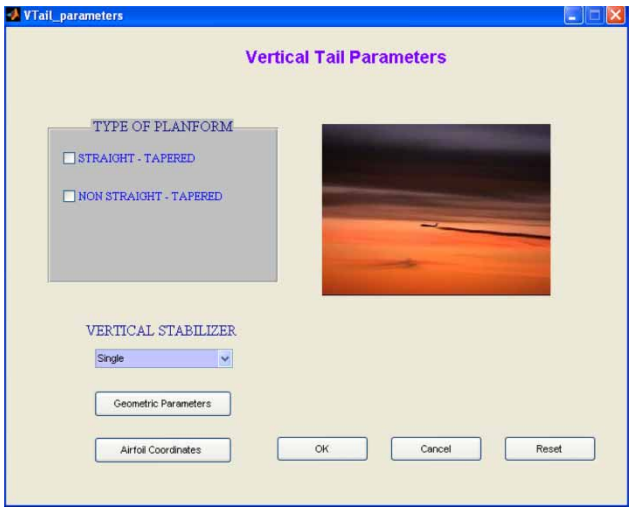

Fig. 5 Vertical tail parameters

parameters and the airfoil co-ordinates situated at the root, MAC, and tip sections are considered. The inputs to the body configuration are the three parameters: fuselage length, position of the gravitational centre, and fuselage co-ordinates (in three dimensions), measured with respect to the reference system.

2.2 FDerivatives: functions' description

The FDerivatives code uses a total of 82 MATLAB functions; the aerodynamic coefficients and their stability derivatives are calculated with 24 of these functions, which are the following:

(a) three functions for lift, drag, and moment coefficient estimation (C_{L}, C_{D}, and C_{m});

(b) six functions for the static derivatives estimation: lift, drag, and pitching moment derivatives due to the angle of attack ($C_{\mathrm{L}\alpha}$, $C_{\mathrm{D}\alpha}$, and $C_{\mathrm{m}\alpha}$), and side-force, yawing, and rolling moments due to the sideslip angle ($C_{y\beta}$, $C_{n\beta}$, and $C_{l\beta}$);

(c) fifteen functions for the estimation of the following dynamic derivatives: lift, drag, and pitching moments due to pitch rate derivatives ($C_{\mathrm{L}q}$, $C_{\mathrm{D}q}$, and $C_{\mathrm{m}q}$); lift, drag, and pitching moments due to angle-of-attack rate derivatives ($C_{\mathrm{L}\dot{\alpha}}$, $C_{\mathrm{m}\dot{\alpha}}$, and $C_{\mathrm{D}\dot{\alpha}}$); side-force, rolling, and yawing moments due to roll-rate derivatives (C_{yp}, C_{lp}, and C_{np}); side-force, rolling, and yawing moment due to yaw rate derivatives (C_{yr}, C_{lr}, and C_{nr}); and side-force, rolling, and yawing moments due to sideslip angle rate derivatives ($C_{y\dot{\beta}}$, $C_{l\dot{\beta}}$, and $C_{n\dot{\beta}}$).

The 58 other functions are needed to calculate the geometrical factors (2D or 3D) and the aerodynamic functions. The main function of the FDerivatives code

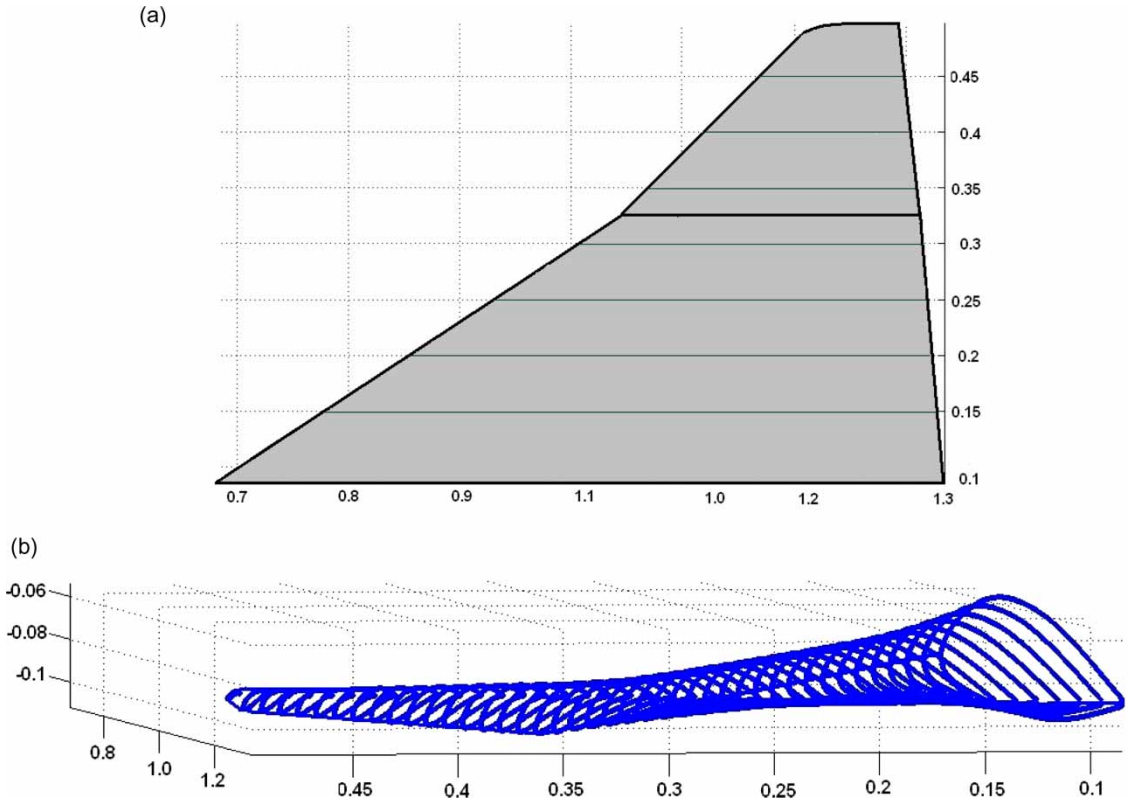

Fig. 6 (a) Wing geometry for X-31 model aircraft and (b) twisted non-linear wing for the X-31 aircraft

is found in the MATLAB file DATCOM.m, which calls the rest of the MATLAB functions and text files. The main functions for the aircraft and airfoils' geometry estimation are aircraft_geometry.m, to determine the wing, canard, vertical tail, and body geometries, and the function airfoil_properties.m which is used to define the geometrical and aerodynamic characteristics of different airfoils (2D and 3D). The zero-lift angle and the pitching moment for a wing section are calculated using thin wing section theory.

The inputs to the body configuration are three global parameters: body length, centre of gravity position at the fuselage station and at the wing level, and the fuselage co-ordinates (in three dimensions). The final numerical results are saved in three formats: jpeg, MATLAB figures, and text files.

2.3 FDerivatives: improvements of the DATCOM method

All of the improvements have been given in detail [**6**, **7**]. Only the improvements that are proposed in the FDerivatives code with respect to the classical DATCOM method are summarized in this article. These improvements are as follows:

(a) lift, drag, and moment coefficients as well as their static and dynamic derivative calculations for the 3D flow around the aircraft;
(b) consideration of several sections across the wing span and their estimations with good precision, found by taking into account the wing root, the MAC, and the tip airfoils (Fig. 6(a));
(c) obtaining of the lift coefficient C_L for a non-linear twist wing (Fig. 6(b));
(d) lift-line-type method is used to obtain the global lift coefficient for a non-linear twist wing [**9**].

The wing lift distribution is calculated using the induced angle of attack for a finite wing span, while the airfoil lift data are calculated at ten wing sections along its span. These ten wing airfoils are found at the root, the MAC, the tip, and seven other intermediate sections. If the airfoil co-ordinates are not all given as inputs, the FDerivatives code has a function that could reconstruct them for any intermediate airfoil.

Table 1 Geometrical parameters

Fuselage length	1.725 m
Wing span	1.0 m
Wing MAC	0.518 18 m
Wing reference area	0.3984 m^2
Wing sweep angle, inboard	57°
Wing sweep angle, outboard	45°
Canard span	0.363 42 m
Canard reference area	0.041 55 m^2
Canard sweep angle	45°
Vertical tail reference area	0.0666 m^2
Vertical tail sweep angle	58°

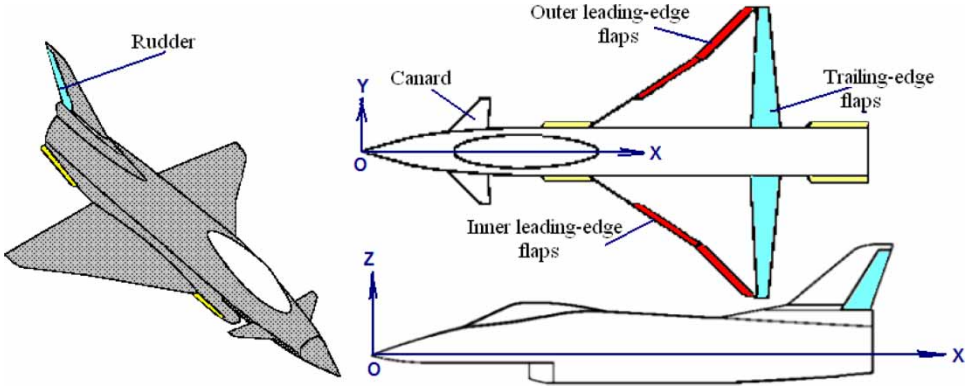

Fig. 7 Three-views of the X-31 model

A lift-distribution method, using successive approximations, is used in the FDerivatives code. For each airfoil section, a section lift coefficient distribution is assumed, for which the 2D lift coefficients are calculated. Equation (1) developed in reference [**10**] is used to estimate the maximum lift coefficient $C_{\mathrm{L}\,\max}$

$$C_{\mathrm{L}\,\max} = \left(\frac{c_{\mathrm{L}}}{c_{\mathrm{L}\,\max}}\right)_{\substack{\theta=0\\ \Lambda=0}} \kappa_{\mathrm{L}\Lambda}(c_{\mathrm{L}\,\max} - \kappa_{\mathrm{L}\theta} C_{\mathrm{L}\alpha}\theta) \tag{1}$$

This method applies to any wing geometry, including to a non-linear twisted wing, and replaces the old algorithm used in the DATCOM method for a linear twisted wing.

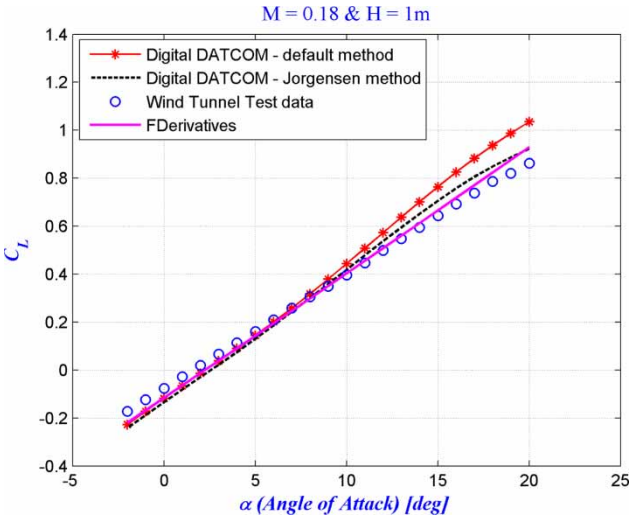

Fig. 8 Lift coefficient variations with angle of attack

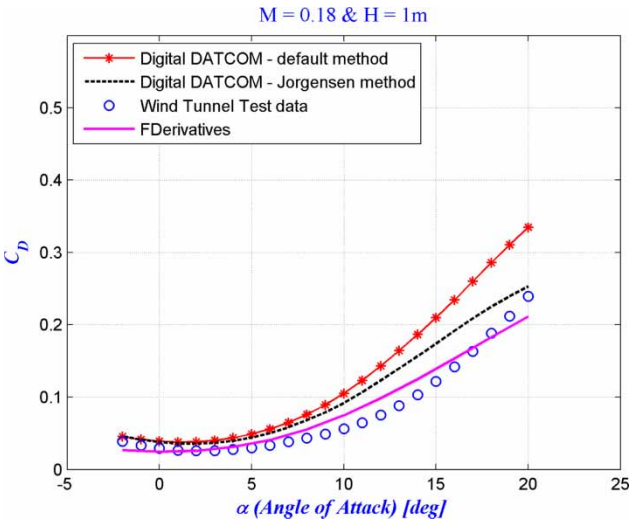

Fig. 9 Drag coefficient variations with angle of attack

Table 2 Relative errors of lift coefficient variation with angle of attack

Alpha (degree)	Digital DATCOM default method (%)	Digital DATCOM Jorgenson method (%)	FDerivatives code (%)
−2	23.930	31.458	20.735
0	19.134	27.578	18.156
2	16.601	23.205	15.012
4	12.838	19.896	14.012
6	4.647	4.441	7.957
8	4.088	4.262	2.075
10	10.674	11.949	1.885
12	12.931	14.852	1.820
14	15.258	18.005	3.079
16	16.128	19.229	3.722
18	16.051	19.120	4.553
20	16.650	19.976	7.197

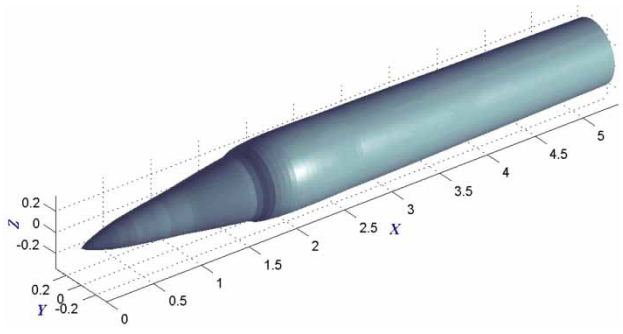

Fig. 10 X-31 aircraft fuselage, modelled as a revolution body

Table 3 Relative errors of drag coefficient variation with angle of attack

Alpha (degree)	Digital DATCOM default method (%)	Digital DATCOM Jorgenson method (%)	FDerivatives code (%)
−2	11.679	9.938	28.286
0	22.071	16.581	12.216
2	32.280	21.749	0.449
4	39.047	24.624	7.670
6	44.470	26.676	11.739
8	50.077	28.596	14.236
10	57.856	30.975	16.498
12	59.603	31.469	15.478
14	53.499	29.681	11.398
16	43.270	26.239	4.901
18	34.429	22.704	2.094
20	26.598	19.012	8.861

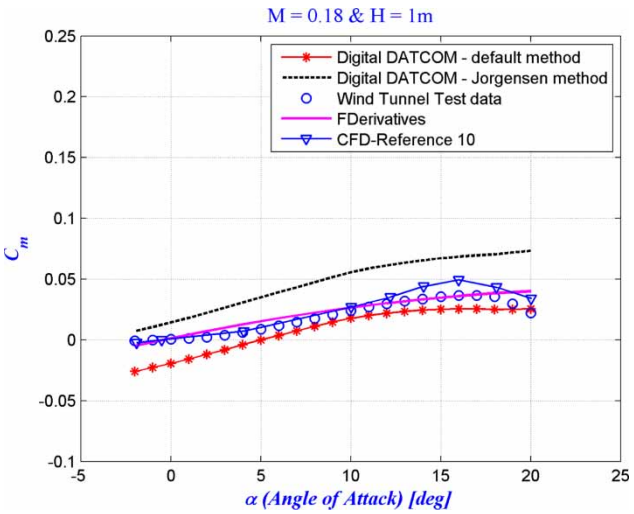

Fig. 11 Pitching moment coefficient variations with angles of attack

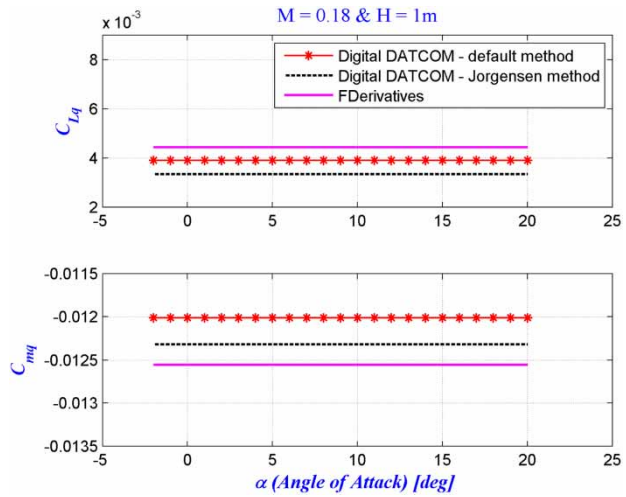

Fig. 12 Lift and pitch moment coefficients due to the pitch rate (C_{Lq}, C_{mq}) versus the angle of attack

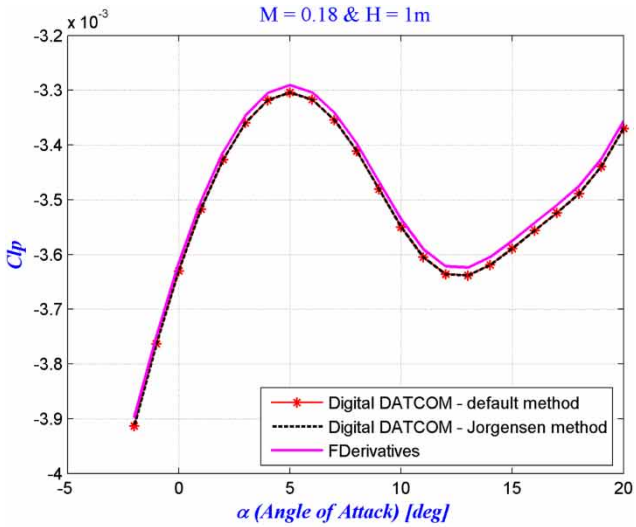

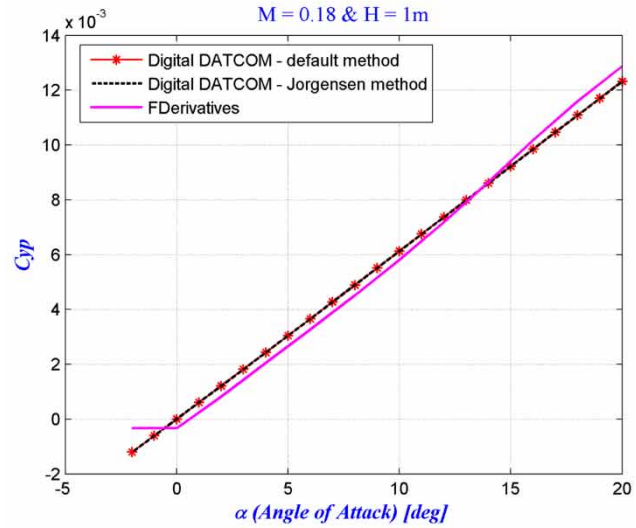

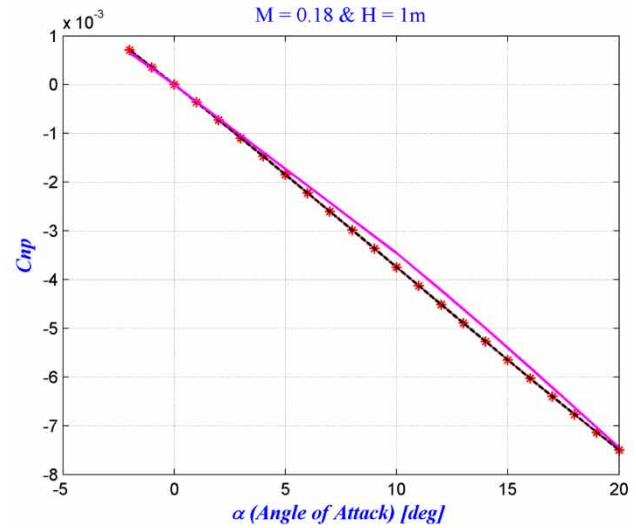

Fig. 13 Yawing, side-force, and rolling moments due to the roll-rate derivatives' variations with the angle of attack

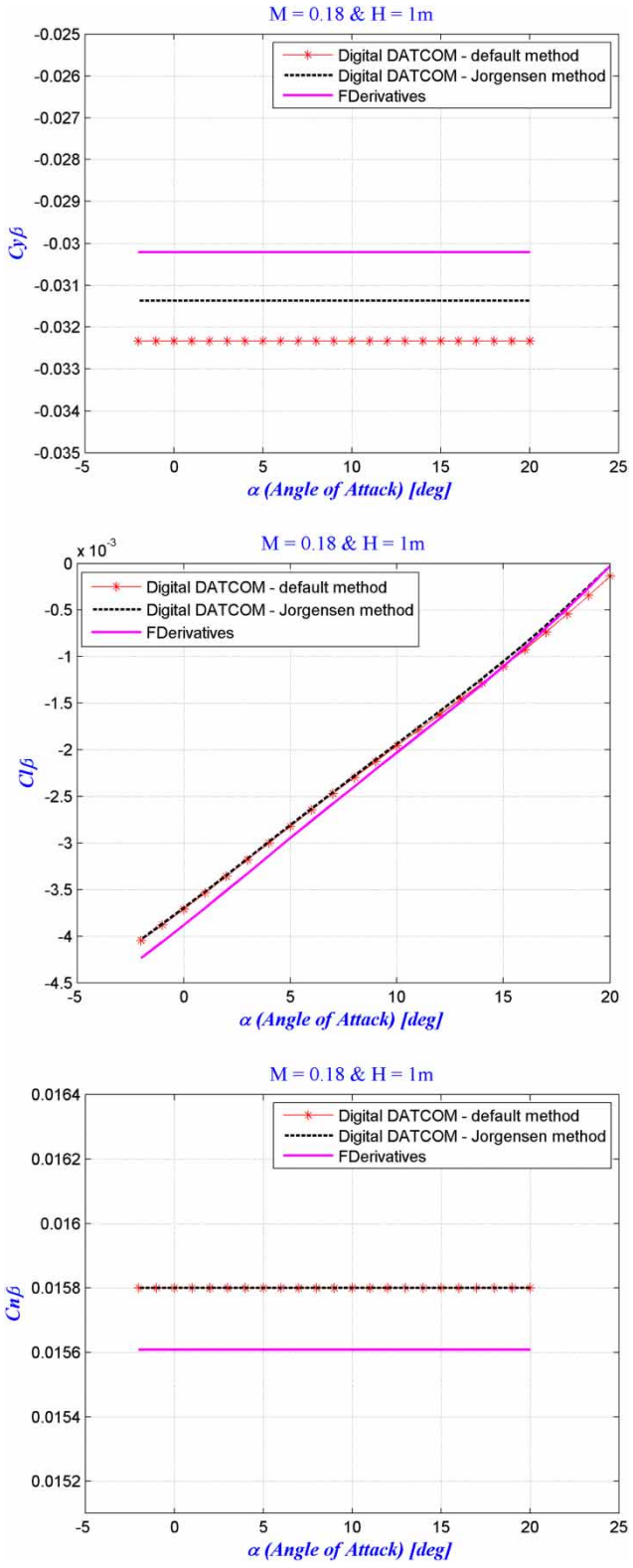

Fig. 14 Side-force, yawing, and rolling moments due to the sideslip angle derivatives' variations with the angle of attack

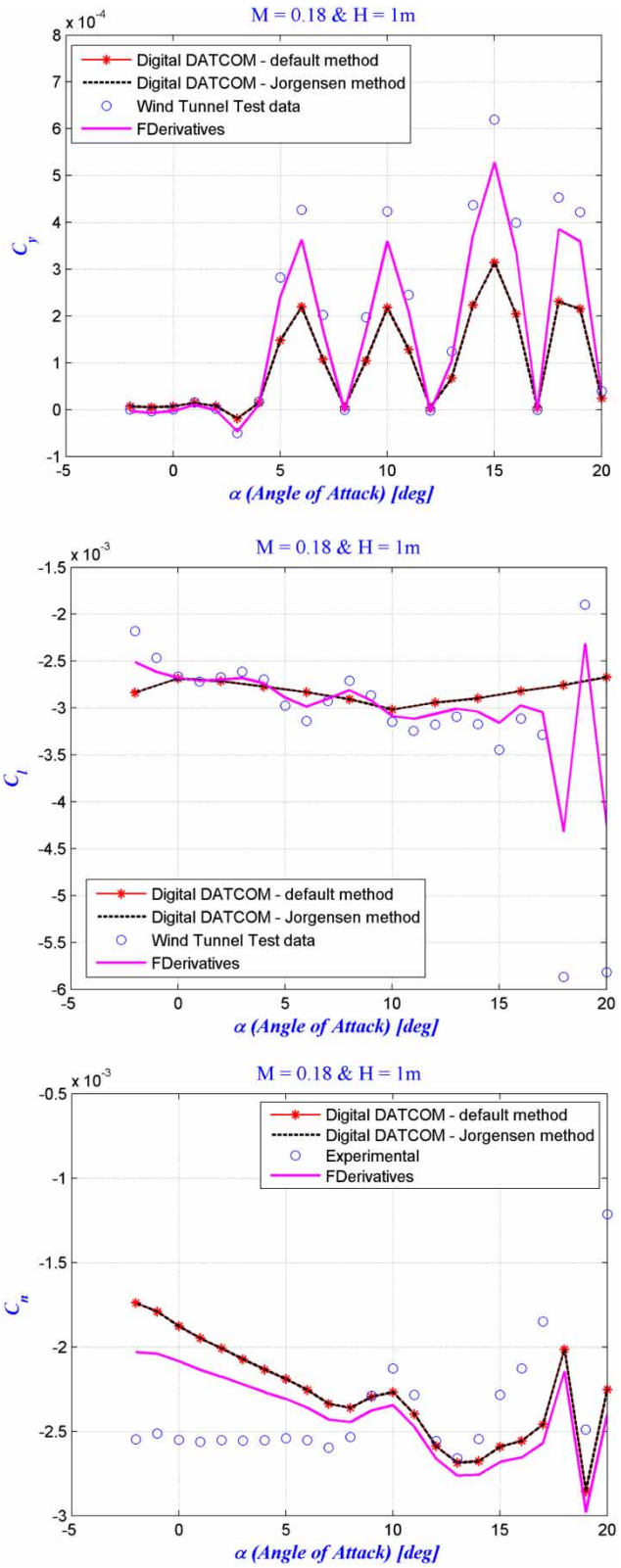

Fig. 15 Side-force, rolling, and yawing moment coefficients variation with angle of attack

The sweep correction factor depends on the aspect and taper ratios, as shown in equation (2)

$$\kappa_{L\Lambda} \cong 1 + \kappa_{\Lambda 1}\Lambda - \kappa_{\Lambda 2}\Lambda^{1.2} \tag{2}$$

The section maximum lift coefficient $c_{L\max}$ used in equation (1) is calculated in the section where the lift coefficient has the highest value. After obtaining the lift distribution along the wing span, the stall

coefficient (corresponding to the maximum lift coefficient) is obtained for the entire wing.

1. With respect to the Digital DATCOM code, the new FDerivatives code, for wing body (WB) configuration, gives better estimation of drag using a nonlinear regression analysis and better estimation of pitching moments.

   This method evaluates and combines the isolated moments due to the lift for the WB configuration, with allowance for their effect on each other. The wing pitching moments due to the effective wing lift include the effects of body up-wash on the wing and of the wing carryover onto the fuselage. Fuselage and nacelles' free moments due to wing-induced flow can be estimated by the technique developed in reference [**11**]. The sum of these two contributions added to the wing pitching moment due to its drag gives a better estimation of the pitching moment than the linear regression analysis method in the Digital DATCOM code for a WB configuration.
2. The zero-lift angle and the pitching moment for a wing section are also calculated with the FDerivatives code using the thin wing section theory [**12**] and the Fourier method. Very good approximations for the zero-lift coefficients and pitching moments are obtained using the Pankhurst method [**12**].

3 TESTING WITH THE X-31 AIRCRAFT MODEL

The X-31 aircraft was designed to break the 'stall barrier', allowing it to fly at angles of attack which would typically cause an aircraft to stall, resulting in loss of control. The X-31employs thrust vectoring paddles which are placed in the jet exhaust, allowing the aircraft's aerodynamic surfaces to maintain their control at very high angles. For its control, the aircraft has a small canard, a single vertical tail with a conventional rudder, and wing leading-edge and trailing-edge flaps.

The X-31 aircraft also uses computer-controlled canard wings to stabilize the aircraft at high angles of attack. The stall angle at low Mach numbers is $\alpha = 30^\circ$. The X-31 model geometry was given by the German Aerospace Centre (DLR), at the scale 1:5.6 (Table 1) in the AVT-161 meeting. The geometrical parameters are detailed [**13**].

The main part of the X-31 model (Fig. 7) is a wing–fuselage section with eight servo-motors for changing the angles of the canard (δ_c), the wing leading-edge inner/outer flaps ($\delta_{LEi}/\delta_{LEo}$), wing trailing-edge flaps (δ_{TE}), and the rudder (δ_r) [**14**]. The variation of these angles, for each control surface, is given as:

(a) canard: $-70^\circ \leqslant \delta_c \leqslant 20^\circ$;
(b) wing inner leading-edge flaps: $-70^\circ \leqslant \delta_{LEi} \leqslant 0^\circ$;
(c) wing outer leading-edge flaps: $-40^\circ \leqslant \delta_{LEo} \leqslant 0^\circ$;
(d) wing trailing-edge flaps: $-30^\circ \leqslant \delta_{TE} \leqslant 30^\circ$;
(e) rudder: $-30^\circ \leqslant \delta_r \leqslant 30^\circ$.

The wing parameters were introduced in Digital DATCOM for the horizontal tail and the canard as a wing.

4 VALIDATION OF THE RESULTS OBTAINED WITH THE X-31 AIRCRAFT

The VN01004 test run was selected from the wind tunnel test data [**13**]. This test took place for angles of attack $\alpha = -6^\circ$ to 55°. The wind tunnel speed was 60 m/s, which corresponds to Mach number 0.18. The Reynolds number based on the MAC value was $Re = 2.07 \times 10^6$, the pressure $P = 101\,045\,\mathrm{N/m^2}$ at temperature $T = 293.7$ K, and the altitude was $H = 1$ m. Results are presented in this article for $\alpha = -2^\circ$ to 20°.

To validate the lift, drag, and moment coefficients obtained with both codes, as shown in Figs 8, 9, and 11, the wind tunnel tests presented in references [**5**], [**13**], and [**15**] were chosen. Both the default method and the Jorgensen method were used for this validation. Jorgensen [**16**] generated a semiempirical method to predict the normal and pitching moment coefficients, as well as the aerodynamic centre position for circular and elliptical bodies with and without wings. Method validity is in the range, for an angle of attack, of 0–90°.

Following the analysis of the results, shown in Figs 8, 9, and 11, one can say that very good approximations were obtained with all methods for the range of angle of attack in the linear zone. Because two codes were used in the article to generate the results, their interpretations are made for two zones: the linear zone and the close-to-stall angle zone.

Table 4 Short-period motion

	$\alpha = 20^\circ$	$\alpha = 28^\circ$	$\alpha = 38^\circ$
λ_{sp} (rad/s)	$-0.8866 \pm 3.5461i$	$-0.4732 \pm 4.3106i$	$-0.7337 \pm 3.6971i$
ω_{nsp} (rad/s)	3.6553	4.3365	3.7692
ς_{sp}	0.2425	0.1091	0.1947
$\begin{Bmatrix} u/V \\ \alpha \\ q \\ \theta \end{Bmatrix}$	$\begin{Bmatrix} 0.1386\angle 74.0162^\circ \\ 1\angle 0^\circ \\ 3.6832\angle 85.2549^\circ \\ 1.0076\angle -18.7821^\circ \end{Bmatrix}$	$\begin{Bmatrix} 0.1640\angle 89.6792^\circ \\ 1\angle 0^\circ \\ 4.5056\angle 92.7223^\circ \\ 1.0390\angle -3.5417^\circ \end{Bmatrix}$	$\begin{Bmatrix} 0.1635\angle 87.1089^\circ \\ 1\angle 0^\circ \\ 3.8826\angle 87.2358^\circ \\ 1.0301\angle -13.989^\circ \end{Bmatrix}$
$\lvert q \rvert$	3.6831	4.5056	3.8827
$\Delta\phi_{sp}$ (degree)	104.0371	96.2641	101.2250

The slopes of the lift coefficient versus the angle of attack are similar, but the closest curve to the experimental results is obtained with the FDerivatives code.

Relative errors were calculated with the classical formula $e = (|x_{\mathrm{WTT}} - x_{\mathrm{calc}}|/x_{\mathrm{WTT}}) \times 100$, where e is the relative error and x_{WTT} is the value obtained in the wind tunnel. The FDerivatives code results are the closest to the wind tunnel test (WTT) results, with a relative error smaller than 18 per cent (see Table 2).

The fuselage was modelled as a body of revolution using the DLR wind tunnel model (see Fig. 10).

For angles of attack between 0° and 20°, the best drag coefficient values are obtained with the FDerivatives (see Fig. 9 and Table 3).

The pitching moment coefficient is very sensitive to geometrical changes and the aircraft's centre of gravity position. Because all the coefficients presented in this article were calculated from the aircraft's geometry, by considering only a small amount of geometrical data as inputs, the final results were not the best when extended for moment coefficients. The curve shapes are similar for the moment coefficient (Fig. 11), but the maximum and minimum values obtained by the default method of Digital DATCOM are higher than the wind tunnel test data. The FDerivatives C_{m} values are better compared with the wind tunnel tests. The main structure of the aircraft, without any approximation (the fuselage is not considered as a revolution body), is modelled using CFD [**5**]. Differences in results are mainly seen for angles of attack between 10° and 20°.

Figures 12 to 14 show the comparison between the stability derivative values obtained with the FDerivatives versus those obtained with the Digital DATCOM codes (default and Jorgensen method).

A very small difference can be seen in Fig. 13 for lift and pitching moment coefficients due to the pitch rate calculated with the FDerivatives and Digital DATCOM codes. Very good results are obtained for yawing and rolling moments and side forces due to roll-rate derivatives (Fig. 14).

Side-force, rolling, and yawing moment coefficients are shown in Fig. 15 with wind tunnel test data [**15**]. These derivatives were calculated based on the aircraft's geometrical data, which imply the occurrence of small errors, and one can see, in Fig. 15, the small side-force coefficient variation with angle of attack with the FDerivatives as well as the Digital DATCOM codes. Very good results were obtained using the FDerivatives codes for rolling and yawing moment coefficients' variation with angle of attack, and the wind tunnel test results (see Fig. 15).

5 LONGITUDINAL MOTION ANALYSIS

This article considers only the aircraft's longitudinal behaviour about the pitch-axis reference frame. The numerical cases are presented here for three high angles of attack, $\alpha = 20°$, 28°, and 38°, based on the previous results.

Let one start from the decoupled equations for longitudinal motion with commands fixed. An aircraft's mathematical model for longitudinal motion can be

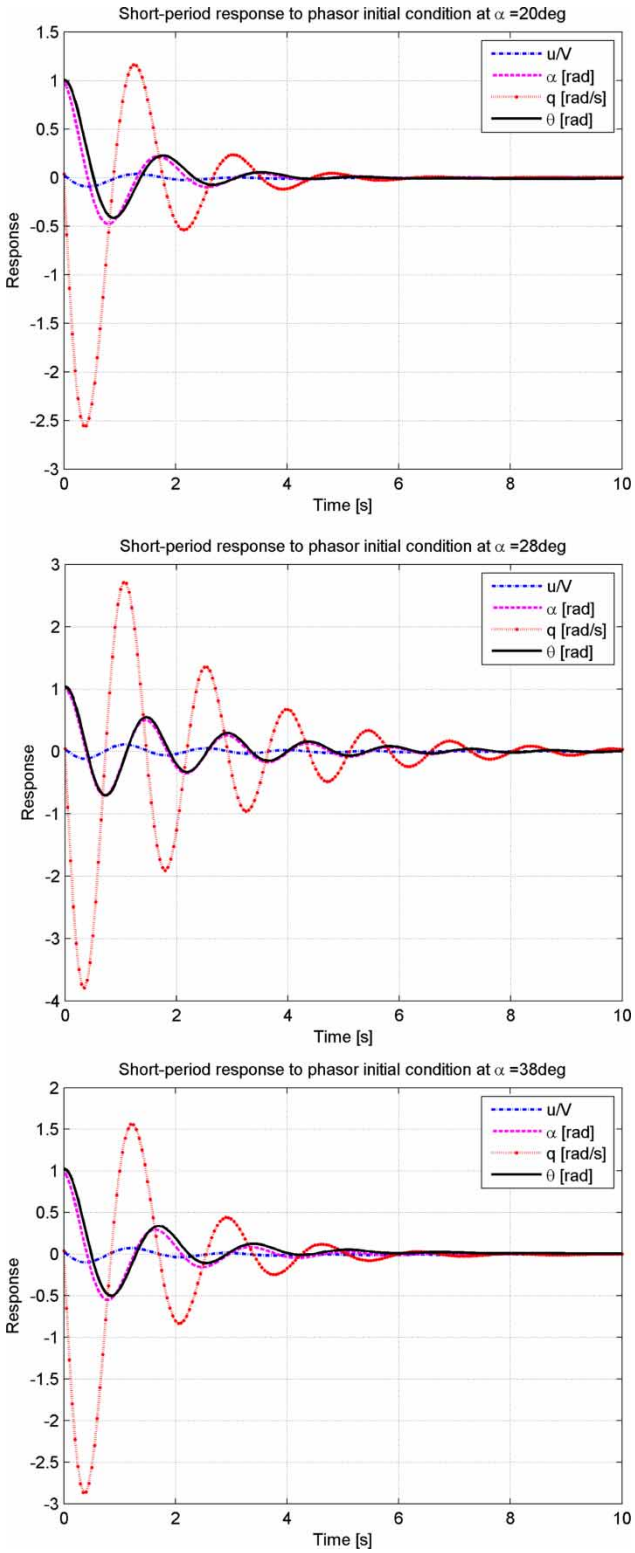

Fig. 16 Short-period response to phasor initial condition

represented by a differential equations system of the form [**17**]

$$\begin{cases} \dfrac{\dot{u}}{V} = X_u\left(\dfrac{u}{V}\right) + \dfrac{X_\alpha}{V} - g\ \cos\ \Theta_0\theta + X_\delta\delta \\ \dot{\alpha} = \dfrac{VZ_u}{V - Z_{\dot{\alpha}}}\left(\dfrac{u}{V}\right) + \dfrac{Z_\alpha}{V - Z_{\dot{\alpha}}}\alpha + \dfrac{V + Z_q}{V - Z_{\dot{\alpha}}}q \\ \qquad - \dfrac{q}{V - Z_{\dot{\alpha}}}\ \sin\ \Theta_0\theta + Z_\delta\delta \\ \dot{q} = \left(VM_u + \dfrac{VZ_uM_{\dot{\alpha}}}{V - Z_{\dot{\alpha}}}\right)\left(\dfrac{u}{V}\right) + \left(M_\alpha + \dfrac{Z_\alpha M_{\dot{\alpha}}}{V - Z_{\dot{\alpha}}}\right)\alpha \\ \qquad + \left(M_q + M_{\dot{\alpha}}\dfrac{V + Z_q}{V - Z_{\dot{\alpha}}}\right)q + M_\delta\delta \\ \dot{\theta} = q \end{cases} \tag{3}$$

If a longitudinal state vector is defined by $\boldsymbol{x} = [u/V\ \alpha\ q\ \theta]^{\mathrm{T}}$ along with a single control term (δ), then the linearized airframe longitudinal dynamics becomes

$$\dot{\boldsymbol{x}} = \mathbf{A}\boldsymbol{x} + \mathbf{B}\delta \tag{4}$$

where **A** is the longitudinal air-frame plant matrix and **B** is the control matrix.

The two pairs of complex conjugate roots of the linearized longitudinal dynamics correspond to short-period (fast mode) and phugoid motions (slow mode). The homogeneous form of equation (4) is given by

$$\dot{\boldsymbol{x}} = \mathbf{A}\boldsymbol{x} \tag{5}$$

The following assumptions are done $H = \text{const}$, $V = \text{const}$ ($M = \text{const}$), $\gamma = 0$ and the calculation conditions are at $H = 1\,\text{m}$ and $M = 0.18 \rightarrow a = 340.2885\,\text{m/s}$, $\rho = 1.2249\,\text{kg/m}^3$.

The set of the first-order linear differential order was solved for short-period and phugoid motions. The short-period motion involves rapid changes to the angle of attack and pitch attitude at roughly constant airspeed. This mode is usually highly damped. Its frequency and damping are very important in the assessment of aircraft handling. In Table 4 numerical results of the short period are given as eigenvalues, modal damping, natural frequency, magnitude and phasing, magnitude scaling, and phase angle difference.

The pitch attitude appears smaller in magnitude as the angle of attack. A time-history trace of the short-period response due to an initial condition of the eigenvector is shown in Fig. 16. The angle of attack and pitch attitude responses are nearly the same for all three angles of attack. For angles of attack equal to 20° and 38° the response becomes stable at 7 s, but for a value of angle of attack close to the stall angle the stabilization time is more than 10 s.

The phugoid mode involves a trade-off between kinetic and potential energy. In this mode, the aircraft, at nearly constant angle of attack, climbs and slows, then dives, losing altitude while picking up speed (Table 5).

The angle-of-attack component is smaller than the u/V component. For this reason, a modal approximation would typically be based on the assumption that the oscillation occurs with the aircraft remaining at a constant lift coefficient. The time-history response is shown in Fig. 17.

The stabilization time differs for the three cases. The longest time is for $\alpha = 20°$, up to 50 s; after that it diminishes until the 20 s for $\alpha = 38°$, and between them the time of 30 s corresponds to $\alpha = 28°$.

The system's control response has been investigated using a step control input. The mathematical model which describes the short-period approximation is given by equation (6)

$$\begin{cases} \dot{\alpha} = \dfrac{Z_\alpha}{V}\alpha + q + \dfrac{Z_\delta}{V}\delta \\ \dot{q} = \left(M_\alpha + \dfrac{Z_\alpha M_{\dot{\alpha}}}{V}\right)\alpha + (M_q + M_{\dot{\alpha}})q \\ \qquad + \left(M_\delta + \dfrac{Z_\delta M_{\dot{\alpha}}}{V}\right)\delta \end{cases} \tag{6}$$

The control input is a step elevator input with the form given by equation (7)

$$\delta_e(t) = \delta_0(t) = \begin{cases} 0, & \text{for } t < 0 \\ \delta_0, & \text{for } t > 0 \end{cases} \tag{7}$$

Table 5 Phugoid motion

	$\alpha = 20°$	$\alpha = 28°$	$\alpha = 38°$
λ_{p} (rad/s)	$-0.1171 \pm 0.3643i$	$-0.2521 \pm 0.3491i$	$-0.3936 \pm 0.1624i$
$\omega_{n\mathrm{p}}$ (rad/s)	0.3826	0.4306	0.4258
ς_{p}	0.3060	0.5854	0.9244
$\begin{Bmatrix} u/V \\ \alpha \\ q \\ \theta \end{Bmatrix}$	$\begin{Bmatrix} 1\angle 0° \\ 0.0434\angle -146.717° \\ 0.9069\angle -2.3979° \\ 2.3701\angle -110.2176° \end{Bmatrix}$	$\begin{Bmatrix} 1\angle 0° \\ 0.0296\angle -137.3727° \\ 1.1276\angle -0.3939° \\ 2.6188\angle -126.2279° \end{Bmatrix}$	$\begin{Bmatrix} 1\angle 0° \\ 0.0221\angle -145.4172° \\ 1.1167\angle -0.4837° \\ 2.6225\angle -158.062° \end{Bmatrix}$
$\lvert q\rvert$	0.9068	1.1277	1.1167
T_{p} (s)	17.2489	17.9992	38.6864

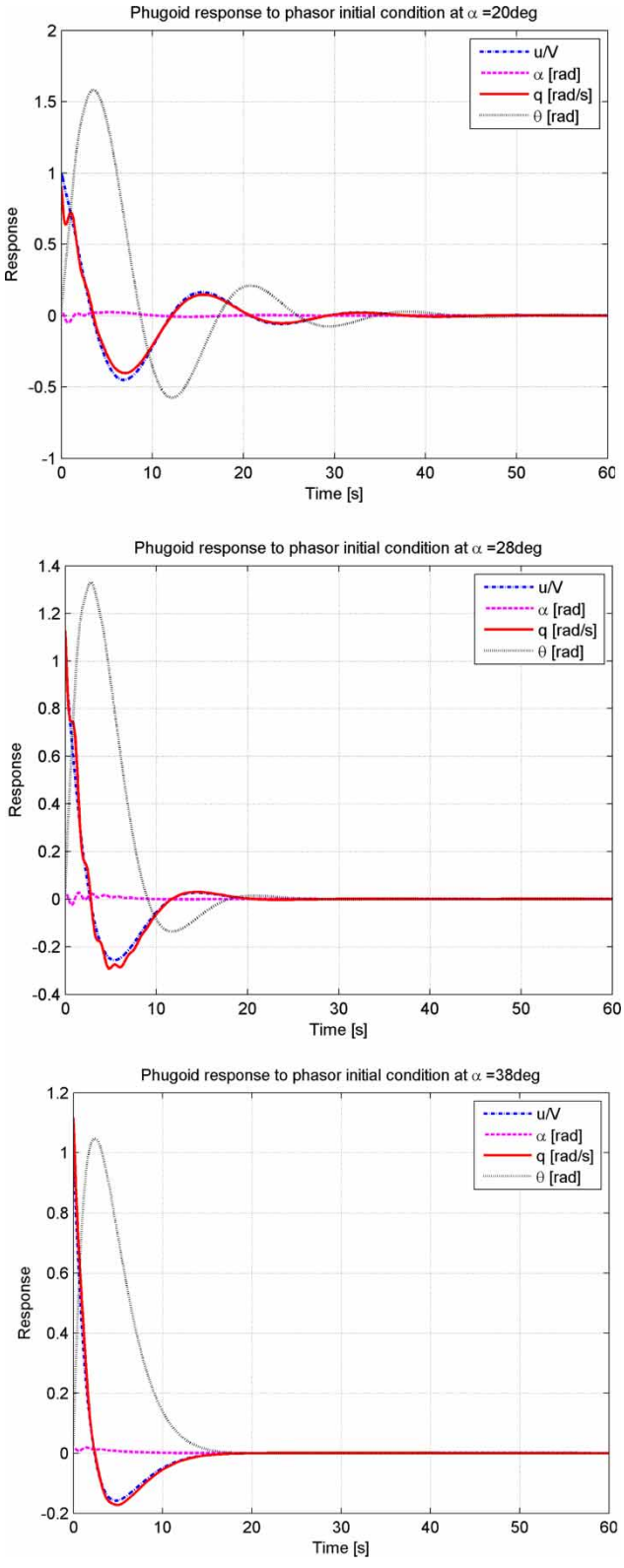

Fig. 17 Phugoid response to phasor initial condition

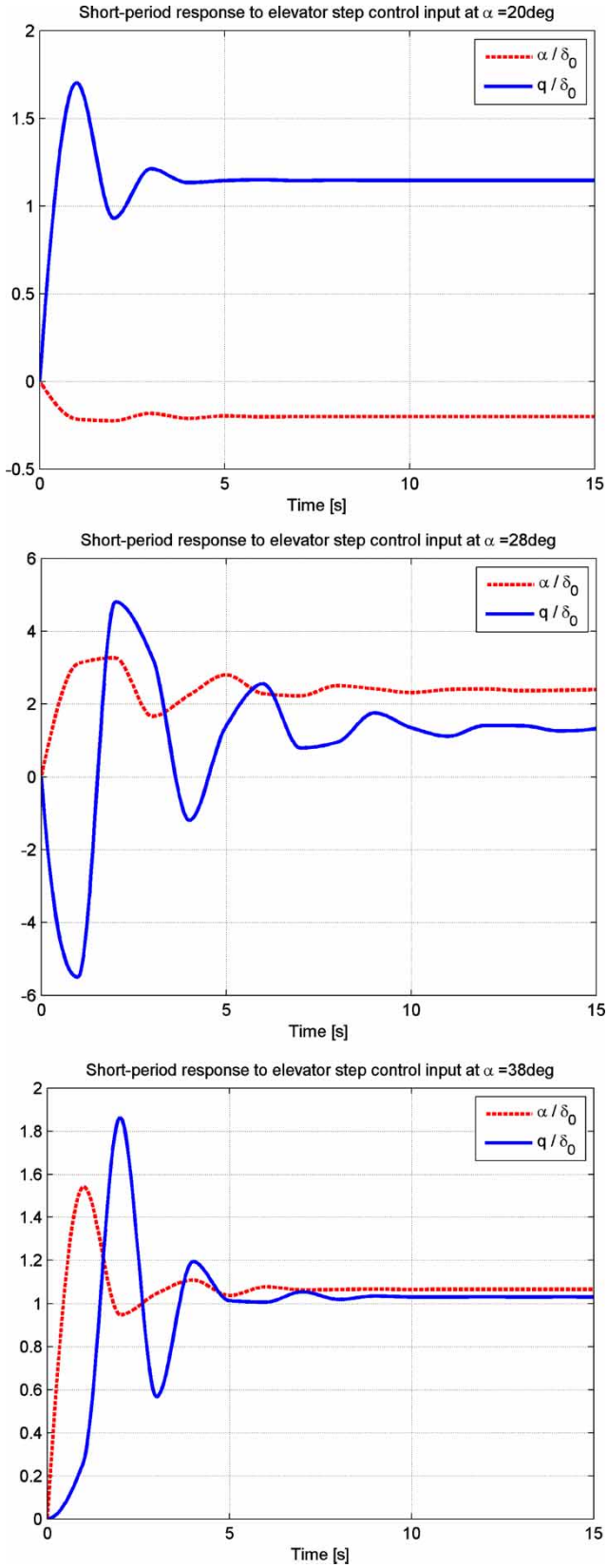

Fig. 18 Short-period response to elevator step input

The time-history plots of α/δ_0 and q/δ_0 are shown in Fig. 18, for time varying from $t = 0$ to 10 s for $\alpha = 20^\circ$ and 38°, and from $t = 0$ to 15 s for $\alpha = 28^\circ$. The stabilized values are shown in Table 6.

The positive elevator deflection corresponds to the trailing edge moving down, which normally results in negative values for both parameters (α and q) when the aircraft is stable. Based on the short-period approximation results, the conclusion is that the X-31 aircraft is not stable for these three angles of attack.

Table 6 Static values for short-period approximation

	$\alpha = 20^\circ$	$\alpha = 28^\circ$	$\alpha = 38^\circ$
α/δ_0 (rad/rad)	−0.2018	2.3857	1.0657
q/δ_0 (rad/rad s)	1.1459	1.3313	1.0308

6 CONCLUSIONS

The aerodynamic coefficients of the X-31 model aircraft and their stability derivatives were calculated based on its geometrical data. The codes used to analyse the model were the classical Digital DATCOM and the FDerivatives codes developed at LARCASE laboratory. Following the AVT-168 meeting, the run test VN01004 ($M = 0.18$, $Re = 2.07 \times 10^6$, $P = 101\,045\,\mathrm{N/m^2}$, and $T = 293.7\,\mathrm{K}$) performed in the low-speed wind tunnel of the German–Dutch Wind Tunnels (DNW–NWB) was used.

By taking into account the small number of geometrical parameters, the remaining geometrical data were calculated to complete the aircraft's geometry knowledge. The fuselage was modelled as a body of revolution and the wing was considered as an equivalent straight tapered platform.

Proper geometry modelling is essential to obtain correct aerodynamic coefficients and their derivatives. Pitching moment coefficient analysis demonstrates how a correct approximation of the aircraft's geometry could be obtained. Lift, drag, and pitching moment coefficients, for angles of attack between -2° and 20°, were calculated with very good accuracy by the FDerivatives code. In addition, rolling and yawing moment coefficients and side-force coefficients were well estimated.

For short-period motion the pitch attitude appears smaller in magnitude than the angle of attack. The angle of attack and pitch attitude responses are nearly the same for all three angles of attack. For angles of attack of 20° and 38° the response becomes stable at 7 s, but for a value of angle of attack close to stall angle the stabilization time is more than 10 s.

A modal approximation would typically be based on the assumption that the oscillation occurs with the aircraft remaining at a constant lift coefficient.

Based on the short-period approximation results, the conclusion is that the X-31 aircraft is not stable for these three angles of attack.

ACKNOWLEDGEMENTS

Thanks are due to Dr Andreas Schütte from DLR and Dr Russell Cummings from the USAF Academy for their leadership and support in RTO/AVT–161 'Assessment of Stability and Control Prediction Methods for NATO Air and Sea Vehicles' and for providing the wind tunnel test data for the X-31 aircraft. In addition, the authors would like to thank Mr Frederic Lidove for his support in the implementation of the MATLAB functions in the FDerivatives code.

REFERENCES

1 **Yeh, D. T., George, M. W., Clever, W. C., Tam, C. K.,** and **Woan, C. J.** Numerical study of the X-31 high angle-of-attack flow characteristics. In Proceedings of the AIAA 22nd Fluid Dynamics, Plasma Dynamics & Lasers Conference, Honolulu, Hawaii, 24–26 June 1991, AIAA paper 91-1630.

2 **Croom, M. A., Fratello, D. J., Whipple, R. D., O'Rourke, M. J.,** and **Trilling, T. W.** Dynamic model testing of the X-31 configuration for high-angle-of-attack flight dynamics research. In Proceedings of the Flight Mechanics Conference, Monterey, California, 9–11 August 1993, AIAA paper 93-3674-CP.

3 **Williams II, D. L.** and **Nelson, R. C.** An investigation of X-31 roll characteristics at high angle-of-attack through subscale model testing. In Proceedings of the 32nd Aerospace Sciences Meeting & Exhibit, Reno, Nevada, 10–13 January 1994, AIAA paper 94-0806.

4 **Cobleigh, B. R.** High-angle-of-attack yawing moment asymmetry of the X-31 aircraft from flight test. NASA Contractor Report 186030, 1994, pp. 1–36.

5 **Boelens, O. J.** CFD analysis of the flow around the X-31 aircraft at high angle of attack. In Proceedings of the 27th AIAA Applied Aerodynamics Conference, San Antonio, Texas, 22–25 June 2009, AIAA paper 2009-3628-968.

6 **Anton, N., Botez, R. M.,** and **Popescu, D.** New methodologies for aircraft stability derivatives determination from its geometrical data. In Proceedings of the AIAA Atmospheric Flight Mechanics Conference, Chicago, Illinois, 10–13 August 2009, AIAA paper 2009-6064.

7 **Popescu, D.** *Nouvelle implémentation de la procédure DATCOM pour le calcul des coefficients aérodynamiques et des dérivées de stabilité dans le domaine subsonique de vol*. Master Thesis, ETS Montréal, 2009.

8 The USAF Stability and Control Digital DATCOM – AFFDL–TR–79–3032.

9 **Sivells, J. C.** and **Neely, R. H.** Method for calculating wing characteristics by lifting-line theory using nonlinear section lift data. NACA-TN-1269, Washington, April 1947.

10 **Phillips, W. F.** and **Alley, N. R.** Predicting maximum lift coefficient for twisted wings using lifting-line theory. *AIAA J. Aircr.*, 2007, **44**(3), 898–910.

11 **Multhopp, H.** Aerodynamics of the fuselage. NACA-TM-1036, Washington, December 1942, pp. 1–47, available from http://naca.central.cranfield.ac.uk/reports/1942/naca-tm-1036.pdf.

12 **Abbot, I. H.** and **von Doenhoff, A. E.** *Theory of wing sections*, 1959 (Dover Publication Inc., New York).

13 **Henne, U., Höhler, G., Klein, C., Rein, M., Sachs, W.,** and **Schütte, A.** Steady state pressure measurements using PSP – 'pressure sensitive paint' and PSI pressure tubes, as well as forces and moments measurements of the X-31 configuration in the low speed wind tunnel

Braunschweig DNW-NWB. DLR IB_224-2005_A16, DLR, 23 September 2005.

14 **Rein, M., Höhler, G., Schütte, A., Bergmann, A.,** and **Löser, T.** Ground-based simulation of complex manoeuvres of a delta-wing aircraft. In Proceedings of the 24th AIAA Aerodynamic Measurement Technology and Ground Testing Conference, San Francisco, 5–8 June 2006, available from http://pdf.aiaa.org/preview/CDReadyMATGT06_1185/PV2006_3149.pdf

15 **Schütte, A.** *X-31 integral PSI steady state plots*, 2009, pp. 25–121 (DLR, Braunschweig).

16 **Jorgensen, L. H.** Prediction of aerodynamic characteristics for slender bodies alone and width lifting surfaces to high angles of attack. AGARD-CP-247, paper 28, 1978.

17 **Schmidt, L. V.** *Introduction to aircraft flight dynamics*, 1998, AIAA Education Series (AIAA, Reston, Virginia).

APPENDIX

Notation

$c_{\mathrm{L\,max}}$	section maximum lift coefficient
C_{D}	drag coefficient
C_{lp}	rolling moment due to the roll-rate derivative
$C_{l\beta}$	rolling moment due to the sideslip angle derivative
C_{L}	lift coefficient
$C_{\mathrm{L}q}$	lift due to the pitch rate derivative
C_{m}	pitching moment coefficient
$C_{\mathrm{m}q}$	pitching moment due to the pitch rate derivative
C_{np}	yawing moment due to the roll-rate derivative
$C_{n\beta}$	yawing moment due to the sideslip angle derivative
C_{yp}	side force due to the roll-rate derivative
$C_{y\beta}$	side force due to the sideslip angle derivative
g	gravity acceleration constant
H	altitude
M	Mach number
M_q	pitching moment due to pitch rate
M_u	pitching moment increment with increased speed
M_α	pitching moment due to the rate of change of the incidence
M_δ	pitching moment due to flaps deflection
t	time
T_p	phugoid mode period
u	forward velocity
V	airspeed
X_u	drag increment with increased speed
X_α	drag due to incidence
X_δ	drag due to flap deflection
Z_q	lift due to pitch rate
Z_u	lift increment due to speed increment
Z_α	lift due to the rate of change of incidence
Z_δ	lift due to flap deflection
α	angle of attack
δ_{c}	canard deflection
δ_{LEi}	wing, leading-edge inner flaps
δ_{LEo}	wing, leading-edge outer flaps
δ_{r}	rudder deflection
δ_{TE}	wing, trailing-edge flaps
ζ_{p}	phugoid natural frequency
ζ_{sp}	short-period natural frequency
θ	total twist (geometrical and aerodynamic)
$\kappa_{\mathrm{L}\theta}$	twist factor in the relation for maximum lift coefficient
$\kappa_{\mathrm{L}\Lambda}$	sweep factor in the relation for maximum lift coefficient
$\kappa_{\Lambda 1}, \kappa_{\Lambda 2}$	twist factor in the relation for maximum lift coefficient
λ_{p}	phugoid eigenvalues
$\omega_{n\mathrm{p}}$	phugoid modal damping
$\omega_{n\mathrm{sp}}$	short-period modal damping